IJMMM International Journal of Minerals, Metallurgy and Materials 矿物冶金与材料学报（英文版）

Effect of Co^{2+} substitution in B-sites of the perovskite system on the phase formation, microstructure, electrical and magnetic properties of $Bi_{0.5}(Na_{0.68}K_{0.22}Li_{0.10})_{0.5}TiO_3$ ceramics

Pamornnarumol Bhupaijit, Chonnarong Kaewsai, Tawat Suriwong, Supree Pinitsoontorn, Surirat Yotthuan, Naratip Vittayakorn, and Theerachai Bongkarn

Cite this article as:
Pamornnarumol Bhupaijit, Chonnarong Kaewsai, Tawat Suriwong, Supree Pinitsoontorn, Surirat Yotthuan, Naratip Vittayakorn, and Theerachai Bongkarn, Effect of Co^{2+} substitution in B-sites of the perovskite system on the phase formation, microstructure, electrical and magnetic properties of $Bi_{0.5}(Na_{0.68}K_{0.22}Li_{0.10})_{0.5}TiO_3$ ceramics, *Int. J. Miner. Metall. Mater.*, 29(2022), No. 9, pp. 1798-1808. https://doi.org/10.1007/s12613-021-2345-8

View the article online at SpringerLink or IJMMM Webpage.

International Journal of Minerals, Metallurgy and Materials
Volume 29, Number 9, September 2022, Page 1798
https://doi.org/10.1007/s12613-021-2345-8

Effect of Co^{2+} substitution in B-sites of the perovskite system on the phase formation, microstructure, electrical and magnetic properties of $Bi_{0.5}(Na_{0.68}K_{0.22}Li_{0.10})_{0.5}TiO_3$ ceramics

Pamornnarumol Bhupaijit[1)], *Chonnarong Kaewsai*[1)], *Tawat Suriwong*[2,3)], *Supree Pinitsoontorn*[4)], *Surirat Yotthuan*[1)], *Naratip Vittayakorn*[5)], *and Theerachai Bongkarn*[1,3),✉]

1) Department of Physics, Faculty of Science, Naresuan University, Phitsanulok 65000, Thailand
2) School of Renewable Energy and Smart Grid Technology, Naresuan University, Phitsanulok 65000, Thailand
3) Research Center for Academic Excellence in Applied Physics, Faculty of Science, Naresuan University, Phitsanulok 65000, Thailand
4) Institute of Nanomaterials Research and Innovation for Energy (IN-RIE), Khon Kaen University, Khon Kaen 40002, Thailand
5) Department of Chemistry, School of Science, King Mongkut's Institute of Technology Ladkrabang, Bangkok 10520, Thailand
(Received: 29 April 2021; revised: 18 August 2021; accepted: 24 August 2021)

Abstract: $Bi_{0.5}(Na_{0.68}K_{0.22}Li_{0.10})_{0.5}Ti_{1-x}Co_xO_3$ lead-free perovskite ceramics (BNKLT–*x*Co, x = 0, 0.005, 0.010, 0.015 and 0.020) were fabricated via the solid-state combustion technique. A small-amount of Co^{2+} ion substitution into Ti-sites led to modification of the phase formation, microstructure, electrical and magnetic properties of BNKLT ceramics. Coexisting rhombohedral and tetragonal phases were observed in all samples using the X-ray diffraction (XRD) technique. The Rietveld refinement revealed that the rhombohedral phase increased from 39% to 88% when x increased from 0 to 0.020. The average grain size increased when x increased. With increasing x, more oxygen vacancies were generated, leading to asymmetry in the bipolar strain (*S*–*E*) hysteresis loops. For the composition of x = 0.010, a high dielectric constant (ε_m) of 5384 and a large strain (S_{max}) of 0.23% with the normalized strain $\left(d_{33}^*\right)$ of 460 pm·V^{-1} were achieved. The BNKLT–0Co ceramic showed diamagnetic behavior but all of the BNKLT–*x*Co ceramics exhibited paramagnetic behavior, measured at 50 K.

Keywords: BNKLT–*x*Co; dielectric; ferroelectric; strain; magnetic

1. Introduction

Pb-based ceramics have globally dominated the field of electro-ceramics, because of their highly efficient electromechanical properties, which are widely used in actuators, sensor and transducers. However, these ceramics possess some serious drawbacks, because of the volatility of the toxic PbO containing compounds during the sintering process in Pb-based ceramics. The toxicity of synthesizing Pb-based ceramics has raised environmental and health concerns [1–3]. Hence, it is essential to examine and develop other environmentally friendly ceramics to replace Pb-based ceramics.

Recently, among many studied lead-free piezoelectric ceramics, for future electronic devices, bismuth sodium titanate $(Bi_{0.5}Na_{0.5})TiO_3$ (BNT) ceramics are considered a potential candidate due to its high Curie temperature (540°C) and large remanent polarization (P_r = 38 μC·cm^{-2}) [4–5]. BNT ceramics though are hard to pole because of its high coercive field (E_c = 73 kV·cm^{-1}) and high electrical conductivity [6–7]. To improve the electrical properties, new research has concentrated on the search for a morphotropic phase boundary (MPB) in BNT-based ceramics [8–9]. Sumang *et al.* [10] reported that the synthesis of the $Bi_{0.5}(Na_{0.68}K_{0.22}Li_{0.10})_{0.5}TiO_3$ system (BNKLT) by the combustion technique with a sintering temperature of 1025°C for 2 h, which led to a MPB composition. It was found that this ceramic exhibited a high dielectric property (ε_m) of 4340 and a high measured density of 5.79 g·cm^{-3}.

Generally, A and B-site acceptor-donor doping causes the atoms to become off-centered and cause lattice distortions in the unit cell, which produces a morphotropic phase boundary (MPB) composition in the system. A number of BNT-based solid solutions were prepared, aiming to obtain a MPB composition, such as $(Bi_{0.5}Na_{0.5})TiO_3$–$(Bi_{0.5}K_{0.5})TiO_3$ (BNKT) [11], $Na_{0.5}Bi_{0.5}TiO_3$–$BaTiO_3$ (BNT–BT) [12] and $(Bi_{0.5}Na_{0.5})TiO_3$–$(Bi_{0.5}K_{0.5})TiO_3$–$(K_{0.5}Na_{0.5})NbO_3$ (BNT–BT–KNN) [13]. More recently our group also observed that substitutions of a transition metal (Fe^{3+}) in B-sites [14] modified $Bi_{0.5}(Na_{0.68}K_{0.22}Li_{0.10})_{0.5}Ti_xFe_{1-x}O_3$ (BNKLT–*x*Fe) ceramics and formed a MPB at this composition, with great ferroelectric properties (P_r = 26.8 μC·cm^{-2}, and E_c = 20.4 kV·cm^{-1}), a maximum strain (S_{max} = 0.20%) and the highest normalized strain (d_{33}^* = 386 pm·V^{-1}) at x = 0.010.

Recently, several researchers have found that the substitu-

✉ Corresponding author: Theerachai Bongkarn E-mail: researchcmu@yahoo.com

tion of Co^{2+} ions into BNT-based systems leads to the coexistence of the rhombohedral and tetragonal phases in the ceramics [15–16]. Thangavelu *et al.* [15] characterized $(Bi_{0.5}Na_{0.5})TiO_3$ ceramics with 5mol% Co^{2+} substituted into Ti sites and showed an increased grain size and unit cell volume, along with Co^{2+} creating oxygen vacancies. Meanwhile, Buntham *et al.* [16] reported that the best values of direct piezoelectric coefficient d_{33} = 105 pC·N^{-1}, a dielectric constant at room temperature ~670, P_r = 16.8 μC·cm^{-2} and E_c = 15.3 kV·cm^{-1} were observed from $(Bi_{0.5}Na_{0.5})(Co_{0.01}Ti_{0.99})O_3$ ceramics. However, research on the transition metal ion Co^{2+} substituted into BNKLT ceramics has not been reported yet, which is very interesting to try to produce a composition at a MPB.

Thus, the present research is aimed at the fabrication of $Bi_{0.5}(Na_{0.68}K_{0.22}Li_{0.10})_{0.5}Ti_{1-x}Co_xO_3$ (abbreviation as; BNKLT–*x*Co) ceramics with different Co^{2+} concentrations between 0.005 and 0.020 mol and to investigate the phase formation with an emphasis on the presence of a MPB. Moreover, the physical, electrical and magnetic properties are examined for this system.

2. Experimental

$Bi_{0.5}(Na_{0.68}K_{0.22}Li_{0.10})_{0.5}Ti_{1-x}Co_xO_3$ (denoted as: BNKLT–*x*Co) ceramics were synthesized by the solid-state combustion techniques. High purity $Bi(NO_3)_3·5H_2O$ (purity ~98.5%), $NaNO_3$ (purity ~99%), KNO_3 (purity ~99%), Li_2CO_3 (purity ~99%), TiO_2 (purity ~99.5%), and $Co(NO_3)_2·6H_2O$ (purity ~99.5%) were selected as starting materials. BNKLT–*x*Co (*x* = 0, 0.005, 0.010, 0.015 and 0.020) powders were weighed and then were milled using zirconia balls in a media of ethanol for 24 h. After milling, these powders were dried and mixed with glycine ($C_2H_5NO_2$) as fuel at a ratio of 1:1.094 by weight. The mixed powders were then calcined in an alumina crucible at 750°C for 2 h [10]. The calcined powders had 3wt% polyvinyl alcohol (PVA) added and were then ball-milled in ethanol for 12. After that, the mixed powders were pressed into disks under a pressure of 80 MPa. Then, the green compacts were sintered in closed alumina crucibles, first at 600°C for 1 h to burn off the binder, and then at 1025°C for 2 h, with a heating rate of 5°C·min^{-1}. In order to measure the electrical properties, silver paste was used to form an electrode on both sides of the polished samples and then fired at 600°C for 30 min.

The phase formation of the BNKLT–*x*Co ceramics were studied using an X-ray diffractometer (XRD, Philips PW 3040/60 X'Pert PRO), using Cu $K_{\alpha1,2}$ (λ = 0.15418 nm) radiation in the scanning range 10° to 70° of 2θ at room temperature. The Rietveld refinement was determined using the Fullprof software. A scanning electron microscope (SEM, Leo, 1455VP) was used to study the microstructure of the BNKLT–*x*Co ceramics after preparing the surface by polishing and thermally etching the ceramics at a temperature of 100°C below the sintering temperature for 15 min. The average grain size of the samples was estimated by the linear intercept method. The grain size distribution was obtained using the ImageJ software and was analyzed by plotting a histogram. The density of sintered BNKLT–*x*Co ceramics was calculated by Archimedes' principle. The measured dielectric properties from 30 to 400°C, in the frequency range of 1 to 100 kHz, was carried out using an LCR meter (HP, 4284A). For ferroelectric and strain properties, all samples were poled in a silicone oil bath with an applied ac field and were measured using a modified Sawyer-Tower circuit (Radiant, PLC2-1014346). In order to verify the true P_r value, the "remanent hysteresis" test was used with electrical pulses (Logic 0 and Logic 1). Logic 0 measures both the switching and non-switching dipole, but Logic 1 measures only the non-switchable dipole in the sample. Thus, subtracting the result of a Logic 1 measurement from a Logic 0 measurement gives the remanent polarization. For the magnetic test, it was studied by a vibrating sample magnetometer (Versa Lab, Quantum Design) at a temperature of 50 K.

3. Results and discussion

3.1. Phase formation

The XRD patterns, measured at room temperature, of BNKLT–*x*Co ceramics with *x* = 0, 0.005, 0.010, 0.015 and 0.020, plotted as a function of 2θ = 10°–70°, are shown in Fig. 1(a). All specimens had a pure perovskite phase and no secondary phase appeared, implying Co^{2+} ions completely diffused into the BNKLT lattice. In order to study the phase transformation from the Co^{2+} ions substituted into B-sites of the BNKLT system, the diffraction peaks in the range of 38°–50° are expanded, as shown in Fig. 1(b). As it is well-known, the pure $Bi_{0.5}Na_{0.5}TiO_3$ and $Bi_{0.5}K_{0.5}TiO_3$ ceramics are characterized by the rhombohedral (JCPDS file No. 036-0340) and tetragonal (JCPDS file No. 036-0339) phases, respectively. Typically, the rhombohedral symmetry is identified by dual peaks of $(003)_R$ and $(021)_R$ in the range of 38°–42° and a single peak of $(200)_R$ in the range of 44°–48°. For the tetragonal symmetry, it presents a single peak of $(111)_T$ (2θ ~38°–42°) and double peaks of $(002)_T$ and $(200)_T$ (2θ ~44°–48°) [10,14]. In Fig. 1(b), it is apparent that the sample with *x* = 0 showed an asymmetrical peak in the range of 38°–42° and dual split peaks of $(002)_T$ and $(200)_T$ at 2θ ~44°–48°, indicating that this sample presented coexisting tetragonal and rhombohedral phases . For the Co^{2+} substituted ceramics, the peaks in the range of 2θ ~38°–42° showed broad peaks in all compositions. For the peaks in the range of 2θ ~44°–48°, the intensity of $(002)_T$ continuously decreased and $(200)_T$ continuously increased, when *x* increased. These results imply that the rhombohedral and tetragonal phases coexist in all specimens and the rhombohedral phase increased with increased *x*.

To identify the phase structure for the BNKLT–*x*Co ceramics precisely, the Rietveld refinement method was employed. Rietveld refinement can be used to measure the structural changes of all the ceramics, to quantify the ratio of the rhombohedral and tetragonal phases, by fitting the XRD

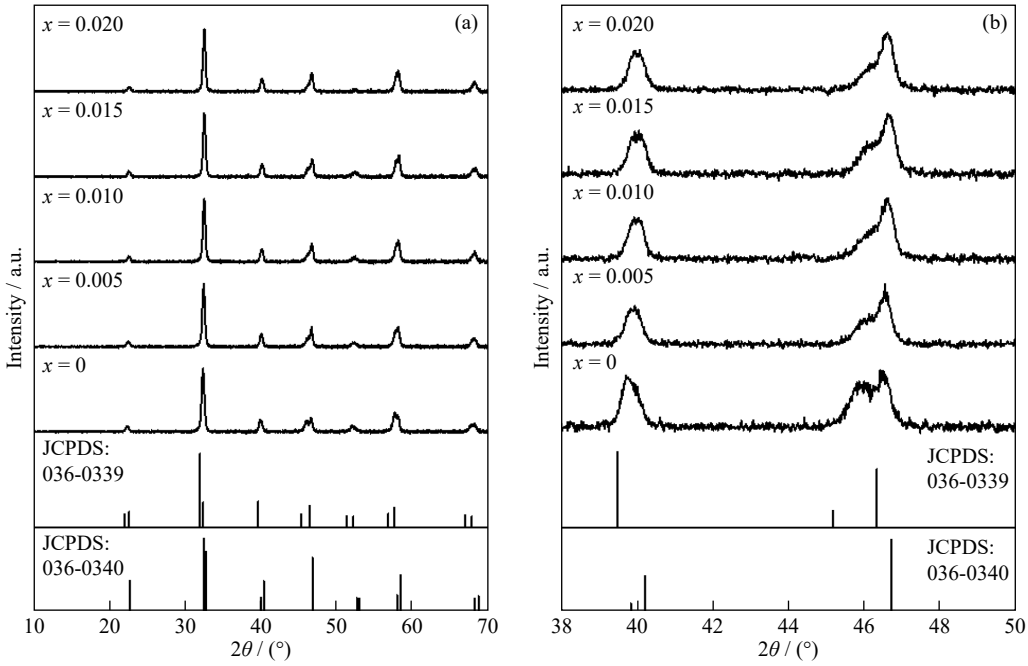

Fig. 1. X-ray diffraction patterns (XRD) of BNKLT–*x*Co ceramics: (a) $2\theta = 10°–70°$; (b) $2\theta = 38°–50°$. JCPDS file No. 036-0339 and 036-0340 were given as the tetragonal and rhombohedral references, respectively.

data with the Fullprof software. The initial values of the lattice parameters, space group and atomic functional positions have been taken from corresponding reference patterns calculated from the Crystallography Open Database (COD). A structural model based on $Bi_{0.5}K_{0.1}Na_{0.4}TiO_3$ with a rhombohedral symmetry using a *R*3*c* space group and a tetragonal symmetry using a *P*4*bm* space group were used as initial models for refining the BNKLT–*x*Co ceramics XRD data. The background was fitted with a Chebyshev polynomial function and the refined profile shape was explained by a Pseudo-Voigt function [17]. The Rietveld refinement on the XRD patterns of all BNKLT–*x*Co ceramics in the 2θ range from 10°–70° are shown in Fig. 2(a)–(e) and the details of the related parameters, quality values, atomic information and the percentage of each phase are shown in Table 1. The quality of the fitting to experimental results showed the profile reliability (R_p) ≤ 31.8%, the weighed pattern reliability (R_{wp}) ≤ 32.9%, the expected residual (R_{exp}) ≤ 17.79% and the goodness of fit (χ^2) ≤ 3.93, all indicated a good agreement with the calculated parameter profiles for all ceramics. The fitting results confirmed that all ceramics had coexisting rhombohedral and tetragonal phases, with an increased rhombohedral phase as *x* increased. Moreover, we can conclude that the rhombohedral and tetragonal phases are close to equal at *x* = 0.010 for BNKLT–*x*Co ceramics and this composition had a phase ratio of rhombohedral: tetragonal = 55:45.

3.2. Microstructure

The SEM images and histograms of the grain size distributions of BNKLT–*x*Co ceramics with different concentrations of Co^{2+} are illustrated in Fig. 3(a)–(e) and (f)–(j), respectively. For the SEM images, all ceramics showed polyhedral grain shapes. At *x* = 0, large pores formed on the surface and a wide grain size distribution was obtained as seen in Fig. 3(f). As the substitution was increased to *x* = 0.005 and 0.010, the porosity was reduced, and the surface morphology showed a narrower grain size distribution (Fig. 3(g)–(h)). With an increase in *x* at 0.015 and 0.020, fewer pores can be seen at the grain boundaries and the surface morphology consisted of a mixture of small and large grain sizes with a wide size distribution, as shown in Fig. 3(i)–(j). According to the linear intercept method, the average grain size of the BNKLT–*x*Co ceramics with $0 \le x \le 0.015$ had a value around 0.5 μm (Table 2). With an *x* of 0.020, the average grain size rapidly increased (around 0.7 μm). The accelerated grain growth may have resulted from the presence of excessive oxygen vacancies, which contributes to mass transport during the sintering process [18–19]. The substituted of Co^{2+} ions at Ti^{4+} site gives rise to the loss of oxygen from the crystal lattice (oxygen vacancies) [16]. From these considerations, it could be assumed that substitutions into the BNKLT–*x*Co ceramics leads to different ionic valences that can promote the phase transformation and lattice distortions of the BNKLT–*x*Co ceramics. The oxygen vacancy was generated according to Eqs. (1) and (2).

$$Co(NO_3)_2 \cdot 6H_2O \rightarrow CoO + 2.5O_2 + N_2 + 6H_2O \quad (1)$$

$$CoO \xrightarrow[TiO_2]{} Co'_{Ti} + O_o^x + V_o^{\bullet\bullet} \quad (2)$$

where CoO substituted TiO_2 at B-site ions of lattice; $V_o^{\bullet\bullet}$ is oxygen vacancy; O_o^x is oxygen ion at the regular site; Co'_{Ti} is the Co^{2+} occupying Ti^{4+} site.

The measured density of the BNKLT–*x*Co ceramics with *x* of 0, 0.005, 0.010, 0.015 and 0.020 are listed in Table 2. The density increased with increased *x* and reached a maximum value at *x* of 0.010 (5.86 $g \cdot cm^{-3}$) and decreased slightly with *x* > 0.010 (Table 2). It is believed that the highest measured density was mainly affected by the good microstructure

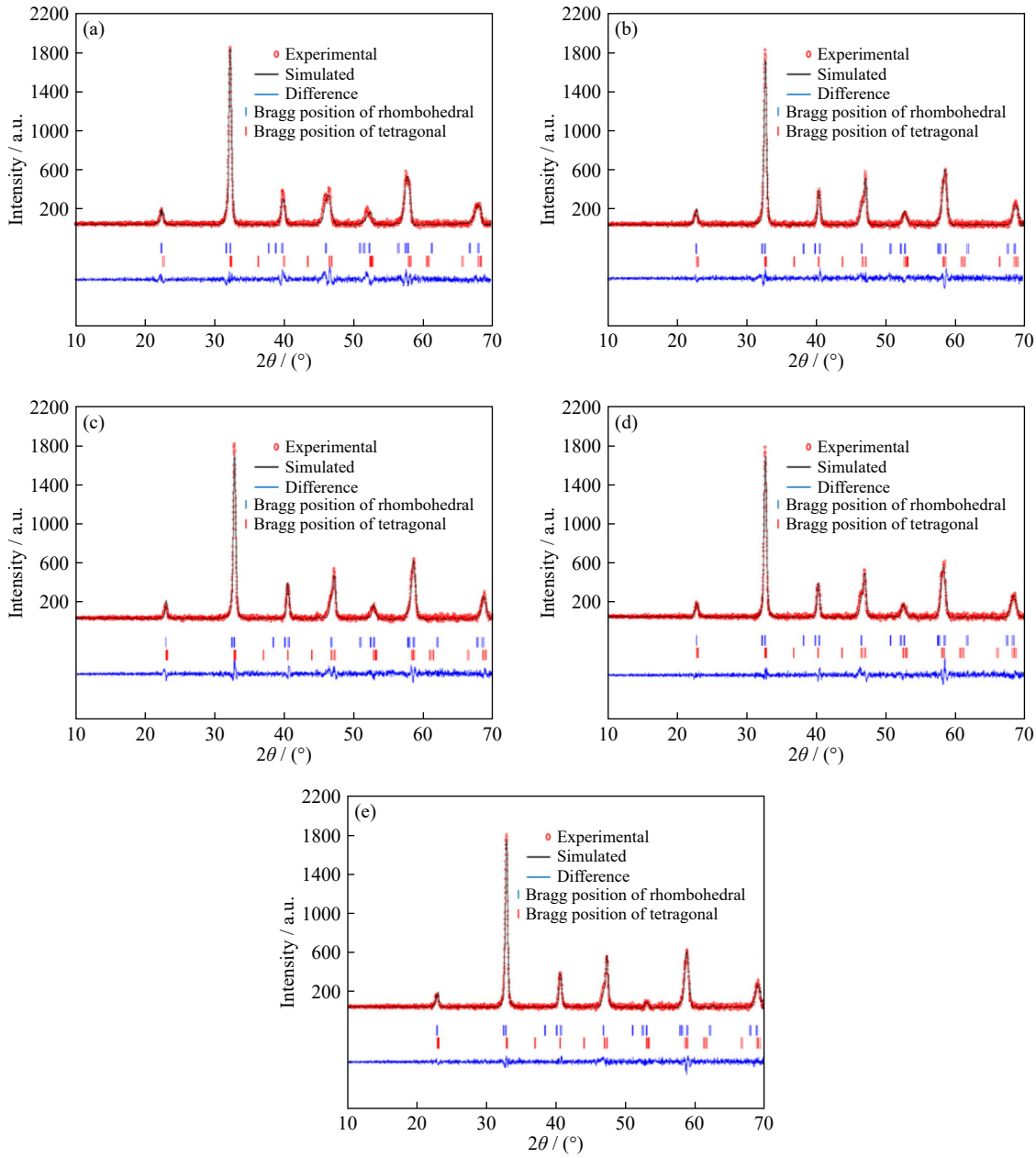

Fig. 2. Rietveld refinement of BNKLT–*x*Co ceramics using rhombohedral (*R*3*c*) and tetragonal (*P*4*bm*) space groups with compositions: (a) $x = 0$; (b) $x = 0.005$; (c) $x = 0.010$; (d) $x = 0.015$; (e) $x = 0.020$.

as seen in the SEM images.

3.3. Dielectric properties

Fig. 4(a)–(e) reveals the temperature dependence of the dielectric properties, as a function of the dielectric constant (left *y*-axis) and dielectric loss (right *y*-axis) measured at 1, 10 and 100 kHz for the BNKLT–*x*Co ceramics. All samples exhibited broad peaks and obvious frequency-dependences, typical of relaxor ferroelectrics. In general, BNT-based ceramics presents two humps (the depolarization temperature (T_d) at a lower temperature and the temperature of maximum dielectric constant (T_m) at a higher temperature). T_d refers to the thermal evolution of polar nano-regions (PNRs) with the *R*3*c* and *P*4*bm* symmetry, which is correlated with the relaxation of PNRs in the rhombohedral phase, while T_m is ascribed to the tetragonal PNRs emerging from the rhombohedral PNRs [14]. At $x = 0$, a T_d around 150°C was found and exhibited a T_m around 349°C (Fig. 4(a)). When $x \geq 0.005$ (Fig. 4(b)–(e)), the T_d became unclear in the curves. Not being able to distinctly observe the T_d may be due to distortions in the lattice parameters [20], indicating a compositionally induced crystal structure change after substitution with Co^{2+} ions. Chen *et al.* [21] reported that an indistinct first dielectric anomaly in the $(Na_xBi_{0.5})_{0.94}Ba_{0.06}TiO_3$ system is influenced by the oxygen vacancies, which corresponds with this work. The T_m value of the BNKLT–*x*Co ceramics reduced from 349 to 342°C when *x* increased from 0 to 0.020. The dielectric constant at T_m (ε_m) of the BNKLT–*x*Co ceramics increased with increased amounts of *x* and reached a maximum value of ε_m of 5384 at $x = 0.010$ and then slightly dropped with a further increase in *x*. This demonstrated that the optimum substitution concentration, for obtaining the highest

Table 1. Lattice parameters, unit cell volume, atomic coordinates and site occupation obtained by Rietveld refinement for the BNKLT–*x*Co ceramics.

Samples	Goodness of fit	Phase structures	Profile parameters	Atoms information					The percentage of phase / %
				Label	*x*	*y*	*z*	Occupancy (Occ.)	
x = 0	χ^2 = 3.93 R_p = 24.6 R_{wp} = 28.1 R_{exp} = 14.17	*R*3*c*	*a* = 0.549848 nm	B	0	0	0.25940	0.47079	39
			c = 1.381039 nm	Na	0	0	0.25940	0.31196	
			c/*a* = 2.51167	K	0	0	0.25940	0.10132	
			u = 1.20921	Li	0	0	0.25940	0.03296	
			v = 0.94582	Ti	0	0	0.25940	0.84270	
			w = –0.23558	O	0.12950	0.32600	0.08330	2.99493	
		*P*4*bm*	*a* = 0.549184 nm	Bi	0	0.5	0.54900	0.50564	61
			c = 0.385401 nm	Na	0	0.5	0.54900	0.31819	
			c/*a* = 0.70177	K	0	0.5	0.54900	0.10637	
			u = 1.68905	Li	0	0.5	0.54900	0.03133	
			v = 1.05383	Ti	0	0	0	0.85114	
			w = –0.22978	O1	0	0	0.52600	2.33577	
				O2	0.26420	0.23570	0.01810	3.17914	
x = 0.005	χ^2 = 3.34 R_p = 31.8 R_{wp} = 32.0 R_{exp} = 17.47	*R*3*c*	*a* = 0.554150 nm	Bi	0	0	0.25940	0.43068	43
			c = 1.331625 nm	Na	0	0	0.25940	0.44167	
			c/*a* = 2.40300	K	0	0	0.25940	0.10450	
			u = 1.20468	Li	0	0	0.25940	0.03226	
			v = 1.15573	Ti	0	0	0.00240	0.88936	
			w = –0.26483	Co	0	0	0.00240	0.00531	
				O	0.12950	0.32600	0.08330	2.97120	
		*P*4*bm*	*a* = 0.544118 nm	Bi	0	0.5	0.54900	0.4437	57
			c = 0.388463 nm	Na	0	0	0.54900	0.31896	
			c/*a* = 0.71393	K	0	0	0.54900	0.10312	
			u = 0.42209	Li	0	0	0.54900	0.03249	
			v = 0.14573	Ti	0	0	0	0.87907	
			w = –0.00906	Co	0	0	0	0.00543	
				O1	0	0	0.52600	2.28257	
				O2	0.26420	0.23570	0.01810	3.58245	
x = 0.010	χ^2 = 3.48 R_p = 31.8 R_{wp} = 32.9 R_{exp} = 17.64	*R*3*c*	*a* = 0.554195 nm	Bi	0	0	0.25940	0.08330	55
			c = 1.336503 nm	Na	0	0	0.25940	0.31874	
			c/*a* = 2.41161	K	0	0	0.25940	0.10587	
			u = 1.38601	Li	0	0	0.25940	0.02122	
			v = –1.00518	Ti	0	0	0.00240	0.84943	
			w = 0.74547	Co	0	0	0.00240	0.01052	
				O	0.12950	0.32600	0.08330	2.20210	
		*P*4*bm*	*a* = 0.545686 nm	Bi	0	0.5	0.54900	0.44656	45
			c = 0.389283 nm	Na	0	0.5	0.54900	0.31915	
			c/*a* = 0.71338	K	0	0.5	0.54900	0.10414	
			u = 0.21243	Li	0	0.5	0.54900	0.03456	
			v = 0.17929	Ti	0	0	0	0.85160	
			w = 0.03257	Co	0	0	0	0.01053	
				O1	0	0	0.52600	2.9456	
				O2	0.26420	0.23570	0.01810	2.74434	
x = 0.015	χ^2 = 3.27 R_p = 29.4 R_{wp} = 31.4 R_{exp} = 17.37	*R*3*c*	*a* = 0.556428 nm	Bi	0	0	0.25940	0.46480	58
			c = 1.340759 nm	Na	0	0	0.25940	0.33049	
			c/*a* = 2.40958	K	0	0	0.25940	0.11050	
			u = 0.84540	Li	0	0	0.25940	0.06114	
			v = 0.87538	Ti	0	0	0.00240	0.87117	
			w = –0.16027	Co	0	0	0.00240	0.01204	
				O	0.12950	0.32600	0.08330	1.71438	

Table 1 (Continued)

Samples	Goodness of fit	Phase structures	Profile parameters	Atoms information					The percentage of phase / %
				Label	*x*	*y*	*z*	Occupancy (Occ.)	
			a = 0.547683 nm	Bi	0	0.5	0.54900	0.37935	
			c = 0.391075 nm	Na	0	0.5	0.54900	0.30685	
			c/a = 0.71405	K	0	0.5	0.54900	0.18260	
		P4bm	u = 0.37120	Li	0	0.5	0.54900	0.06647	42
			v = 0.17933	Ti	0	0	0	0.84071	
			w = 0.01955	Co	0	0	0	0.01441	
				O1	0	0	0.52600	3.00317	
				O2	0.26420	0.23570	0.01810	3.13757	
			a = 0.552747 nm	Bi	0	0	0.25940	0.46969	
			c = 1.331039 nm	Na	0	0	0.25940	0.34424	
			c/a = 2.40804	K	0	0	0.25940	0.10139	
		R3c	u = 0.46770	L	0	0	0.25940	0.03707	88
			v = 1.01955	Ti	0	0	0.00240	0.87645	
			w = –0.20696	Co	0	0	0.00240	0.0218	
	χ^2 = 2.92			O	0.12950	0.32600	0.08330	1.47287	
x = 0.020	R_p = 29.3		a = 0.543765 nm	Bi	0	0.	0.54900	0.39824	
	R_{wp} = 30.4		c = 0.387379 nm	Na	0	0.5	0.54900	0.31920	
	R_{exp} = 17.79		c/a = 0.71240	K	0	0.5	0.54900	0.10146	
		P4bm	u = 0.24455	Li	0	0.5	0.54900	0.03376	12
			v = 0.15342	Ti	0	0	0	0.77816	
			w = 0.01459	Co	0	0	0	0.01417	
				O1	0	0	0.52600	3.04490	
				O2	0.26420	0.23570	0.01810	2.73464	

dielectric constant is an x of 0.010, which resulted from the good phase ratio (near MPB) and the highest density. For the dielectric loss tangent (tanδ) at T_m, it showed a similar value for all x values. The tanδ above T_m sharply increased due to the high conductivity of the ceramics at high temperature (seen in Fig. 4(a)–(e)). Dielectric properties (ε_m and tanδ at T_m) and the T_m of BNKLT–xCo ceramics measured at 1 kHz frequency are listed in Table 2.

3.4. Ferroelectric behavior

Fig. 5 illustrates the polarization (*P*–*E*) hysteresis loops with a normal polarization hysteresis loop (black dots) and remanent polarization hysteresis loop (red dots) and the bipolar strain (*S*–*E*) hysteresis loops of BNKLT–xCo ceramics with x = 0, 0.010 and 0.020. The *P*–*E* hysteresis loops with the normal polarization hysteresis loop procedure refers to the total polarization, including ferroelectric polarization and non-ferroelectric polarization (defect dipole); while, the *P*–*E* hysteresis loops with the remanent polarization hysteresis loop procedure ascribe only ferroelectric polarization, leading to a square-like loop [22]. For the *P*–*E* hysteresis loops produced with the normal polarization hysteresis loop procedure, as shown in Fig. 5(a)–(c), shows all samples exhibited a typical ferroelectric characteristic. Most of the research confirms that BNT-based ceramic is characterize by relaxor ferroelectric behavior [23–24]. For this work, all samples may be non-ergodic relaxor ferroelectrics (NER), which transforms irreversibly into the ferroelectric state under an external electric field. At x lower than 0.010 (Fig. 5(a)–(b)), these ceramics presented well saturated polarization suggesting good poling behavior of the ceramics. However, at x higher than 0.010 (Fig. 5(c)), it showed a relatively large leakage current which may be attributed to excessive oxygen vacancies (Eq. (2)), which corresponded to the earlier parts. The P_r (red dots) increased from 15.6 to 20.8 μC·cm^{-2} when increasing x from 0 to 0.020. For the E_c value (red dots), it decreased from 25.1 to 21.7 kV·cm^{-1} when x increased from 0 to 0.010 and then rapidly increased. The ferroelectric properties (P_r and E_c) are summarized in Table 2.

3.5. Strain behavior

The bipolar strain (*S*–*E*) hysteresis loops of BNKLT–xCo with x = 0, 0.010 and 0.020, under an electric field of 50 kV·cm^{-1}, were obtained and are shown in Fig. 5(d)–(f). All samples showed butterfly-shapes with positive strain (S_{pol}) and negatives strain (S_{neg}). Note that this characteristic reveals NER, which corresponds to the dielectric and ferroelectrics properties. At x = 0 and 0.010 (Fig. 5(a)–(b)), the *S*–*E* loops showed a symmetric shape, while, at x = 0.020, it displayed an asymmetric shape (Fig. 5(c)). The asymmetric shape in the x of 0.020 ceramic is caused by the internal bias field from the excessive oxygen vacancies [25]. In addition, at x = 0.010, both S_{pol} and S_{neg} were enhanced, indicating that this composition becomes softened due to easier domain wall motions. For the maximum strain (S_{max}) with S_{pol} side, the S_{max} value rapidly increased from 0.09% to 0.23% when x in-

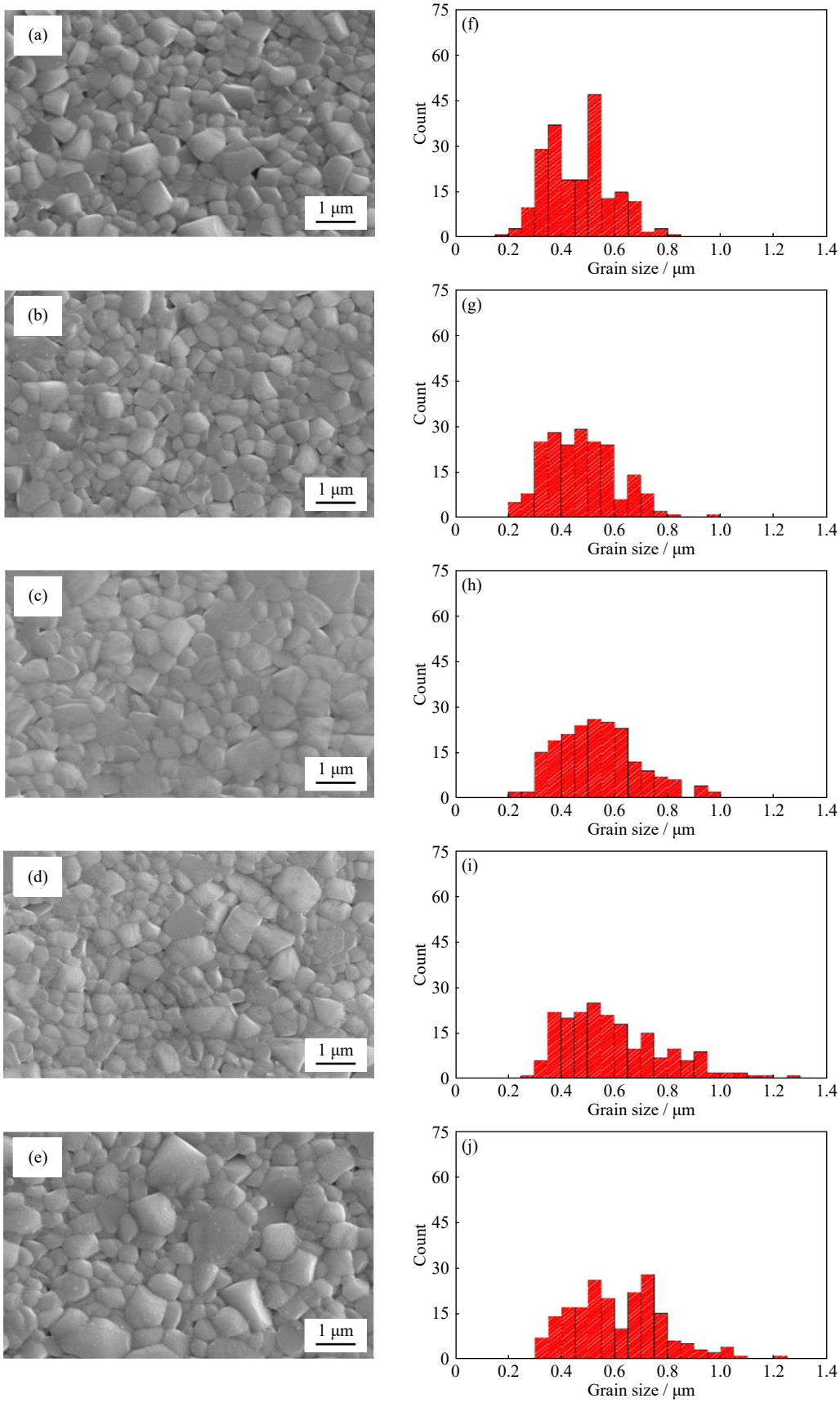

Fig. 3. SEM images and grain size distribution of BNKLT–*x*Co ceramics with (a, f) $x = 0$, (b, g) $x = 0.005$, (c, h) $x = 0.010$, (d, i) $x = 0.015$, and (e, j) $x = 0.020$.

creased from 0 to 0.010, and then decreased as listed in Table 2. The normalized strain (d_{33}^*) is calculated using the equation [26–27],

$$d_{33}^* = S_{max}/E_{max} \tag{3}$$

Table 2. Average grain size, density, dielectric, ferroelectric, strain and magnetic properties of BNKLT–*x*Co ceramics

x	Averagegrain size / μm	Density / (g·cm^{-3})	T_m / °C	ε_m	tanδ at T_m	P_r / (μC·cm^{-2})	E_c/ (kV·cm^{-1})	S_{max} / %	d^*_{33} / (pm·V^{-1})	M_s / (A·m^2·kg^{-1}) (50 K)
0	0.52	5.73	349	4679	0.08	15.6	25.1	0.09	180	–0.0014
0.005	0.52	5.75	348	5144	0.07	15.7	22.5	0.15	300	0.0097
0.010	0.57	5.86	345	5384	0.08	17.8	21.7	0.23	460	0.0202
0.015	0.55	5.81	345	5226	0.07	19.2	29.0	0.17	340	0.0301
0.020	0.71	5.78	342	4800	0.05	20.8	31.4	0.15	300	0.0387

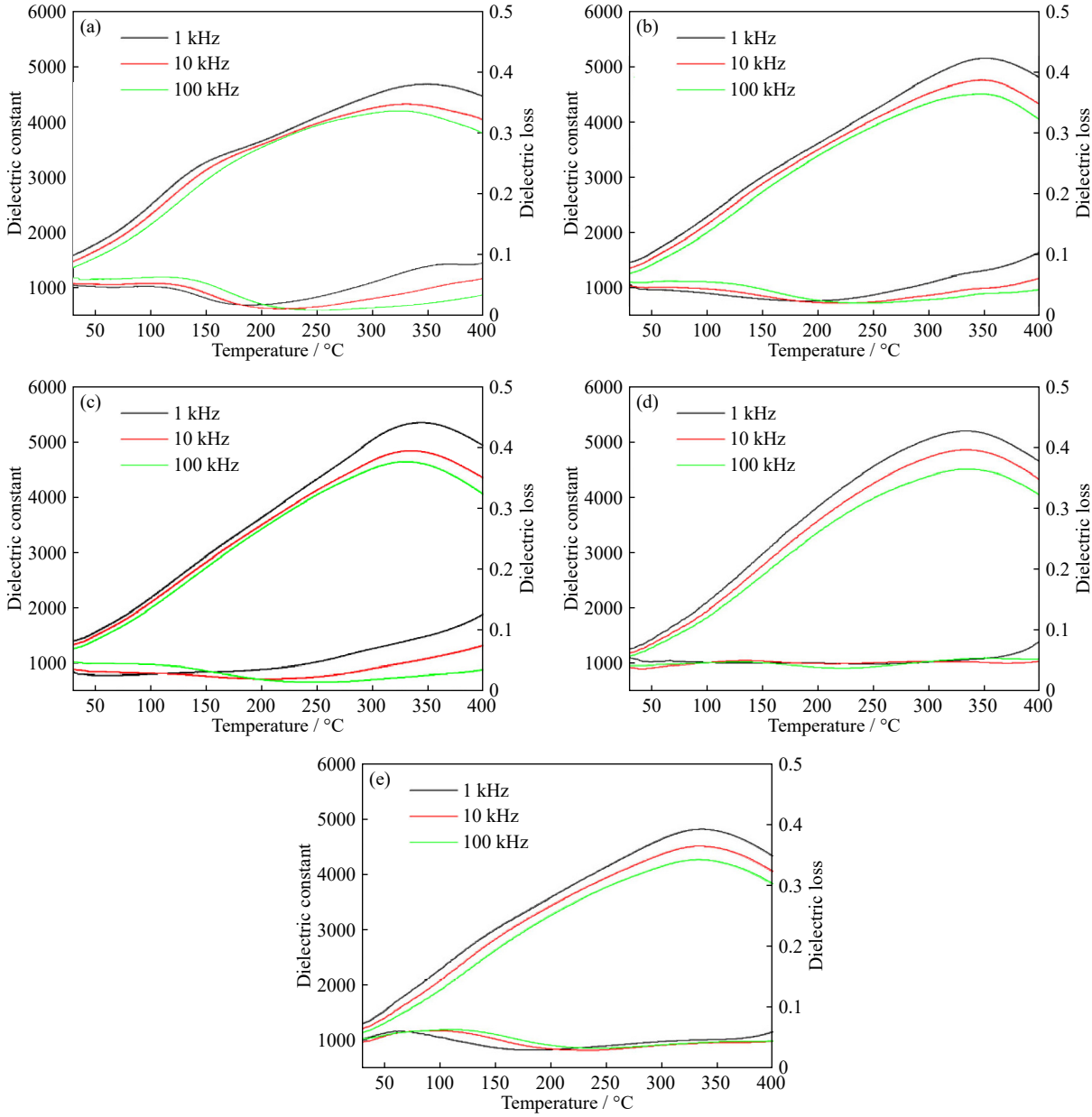

Fig. 4. Dielectric constant and dielectric loss of the BNKLT–*x*Co ceramics with different amounts of Co^{2+} (a) $x = 0$, (b) $x = 0.005$, (c) $x = 0.010$, (d) $x = 0.015$ and (e) $x = 0.020$ as a function of temperature at the frequencies of 1, 10, and 100 kHz.

where S_{max} refers to the highest maximum strain in a sample and E_{max} refers to the maximum applied electric field.

The calculated value of $d^*_{33}$is displayed in Table 2. The $d^*_{33}$of the BNKLT–0Co ceramic was 180 pm·V^{-1}. The d^*_{33} value increased with increased x and reached the maximun value of 460 pm·V^{-1} for the BNKLT–0.010Co ceramic. The d^*_{33} of other modified BNT ceramics present values around 200–400 pm·V^{-1} [9,13,25,28], which are lower than when compared with the BNKLT–0.010Co ceramic in this study.

Excellent dielectric and piezoelectric properties, and suitable ferroelectric properties were demonstrated at $x = 0.010$, implying that this composition is a near MPB region with the rhombohedral and tetragonal phases in a ratio of 55:45 as ob-

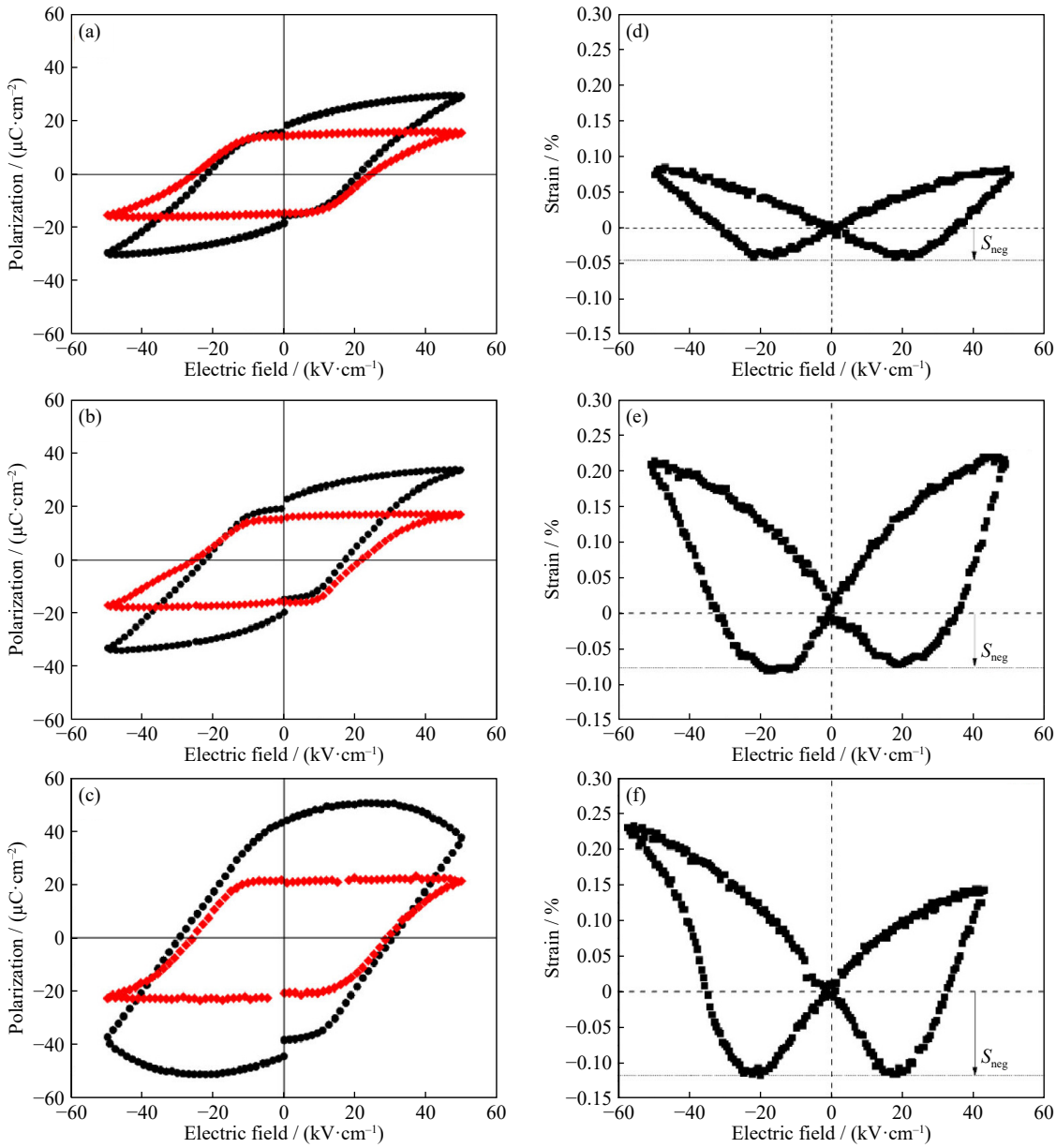

Fig. 5. (a, b, c) Polarization hysteresis loops with normal polarization hysteresis loop (black dot) and remanent polarization hysteresis loop (red dot) and (d, e, f) bipolar strain hysteresis loops (right) measured at room temperature as a function of applied electric field of 50 kV·cm^{-1} of BNKLT–*x*Co ceramics: (a, d) *x* = 0; (b, e) *x* = 0.010; (c, f) *x* = 0.020.

served in the XRD results, with a good microstructure and high density.

3.6. Magnetic properties

Fig. 6 is the results of the application of an alternating magnetic field, which produced a hysteretic magnetization–magnetic field loops (*M*–*H* loops) at 50 K. The BNKLT–0Co ceramic displayed diamagnetic behavior with a negative slope because all the electrons in the 3d-orbital of this composition are paired. When Co^{2+} ions are substituted into the BNKLT system in the 0.005 to 0.020 mol range, the *M*–*H* loops gradually became paramagnetic with a positive slope and the saturated magnetization (M_s) values slightly increased (seen in Table 2), which occurs with increased oxygen vacancies and the associated increase of unpaired 3d-orbitals, from the increased magnetic exchange interaction of the nearest and next nearest neighboring Co^{2+} ions within the unit cell of BNKLT–*x*Co ceramics.

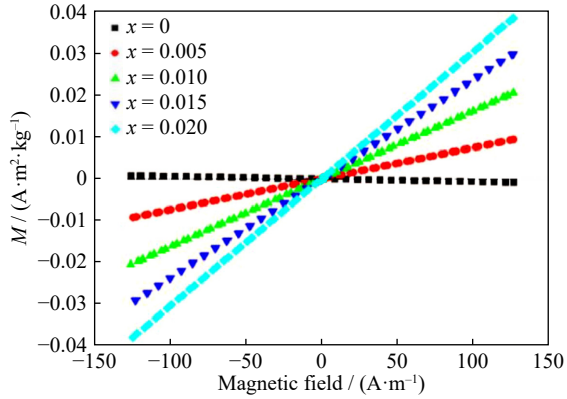

Fig. 6. Magnetic hysteresis loops (*M*–*H* loops) recorded at 50 K for BNKLT–*x*Co ceramics with *x* = 0–0.020.

4. Conclusion

In this work, Co^{2+} ions modified the phase formation, microstructure and electrical properties of $Bi_{0.5}(Na_{0.68}K_{0.22}Li_{0.10})_{0.5}Ti_{1-x}Co_xO_3$ ceramics with x values of 0, 0.005, 0.010, 0.015 and 0.020 mol. The XRD analysis exhibited the coexistence of the tetragonal and rhombohedral phases in all samples and the rhombohedral phase increased from 39% to 88% when x increased from 0 to 0.020. The replacement of Ti^{4+} ions by Co^{2+} ions at B-sites significantly affected the content of oxygen vacancies leading to changes in the microstructure, dielectric, ferroelectric and piezoelectric properties. BNKLT ceramics exhibit diamagnetic behavior. However, upon substituting Co^{2+} ions into BNKLT ceramics, paramagnetic behavior was demonstrated and M_s increased with increased amounts of Co^{2+} ions. The greatest dielectric constant (ε_m), large strain (S_{max}), superior normalized strain (d^*_{33}) and excellent ferroelectric properties (P_r and E_c) of 5384, 0.23%, 460 pm·V^{-1}, 17.8 μC·cm^{-2} and 21.7 kV·cm^{-1}, respectively, were obtained at x = 0.010, which was near a MPB composition with a ratio of rhombohedral: tetragonal of 55: 45. This sample also showed a good microstructure and the maximum density (5.86 g·cm^{-3}).

Acknowledgements

This work was financially supported by the National Science, Research and Innovation Fund (NSRF) through Naresuan University (R2564B001). The authors wish to thank the Department of Physics, Faculty of Science, Naresuan University for their supporting facilities. Thanks are also given to Asst. Prof. Dr. Kyle V. Lopin for his help in editing the manuscript.

Conflict of Interest

The authors declare no conflict of interests.

References

[1] L.X. He, M. Gao, C.E. Li, W.M. Zhu, and H.X. Yan, Effects of Cr_2O_3 addition on the piezoelectric properties and microstructure of $PbZr_xTi_y(Mg_{1/3}Nb_{2/3})_{1-x-y}O_3$ ceramics, *J. Eur. Ceram. Soc.*, 21(2001), No. 6, p. 703.

[2] J.J. Choi, J.H. Lee, B.D. Hahn, W.H. Yoon, and D.S. Park, Co-firing of PZN–PZT/Ag multilayer actuator prepared by tape-casting method, *Mater. Res. Bull.*, 43(2008), No. 2, p. 483.

[3] T. Yamamoto, Ferroelectric properties of the $PbZrO_3$–$PbTiO_3$ system, *Jpn. J. Appl. Phys.*, 35(1996), No. 9S, p. 5104.

[4] J.M. Li, F.F. Wang, C.M. Leung, S.W. Or, Y.X. Tang, X.M. Chen, T. Wang, X.M. Qin, and W.Z. Shi, Large strain response in acceptor- and donor-doped $Bi_{0.5}Na_{0.5}TiO_3$-based lead-free ceramics, *J. Mater. Sci.*, 46(2011), No. 17, p. 5702.

[5] A. Maqbool, A. Hussain, R.A. Malik, A. Zaman, T.K. Song, W.J. Kim, and M.H. Kim, Dielectric and ferroelectric properties of Nb doped BNT-based relaxor ferroelectrics, *Korean. J. Mater. Res.*, 25(2015), No. 7, p. 317.

[6] G.J. Lee, B.H. Kim, S.A. Yang, J.J. Park, S.D. Bu, and M.K. Lee, Piezoelectric and ferroelectric properties of (Bi,Na)TiO_3–(Bi,Li)TiO_3–(Bi,K)TiO_3 ceramics for accelerometer application, *J. Am. Ceram. Soc.*, 100(2016), No. 2, p. 678.

[7] J.H. Cho, Y.H. Jeong, J.H. Nam, J.S. Yun, and Y.J. Park, Phase transition and piezoelectric properties of lead-free $(Bi_{1/2}Na_{1/2})TiO_3$–$BaTiO_3$ ceramics, *Ceram. Int.*, 40(2014), No. 6, p. 8419.

[8] Y.J. Dai, X.W. Zhang, and K.P. Chen, An approach to improve the piezoelectric property of $(Bi_{0.5}Na_{0.5})TiO_3$–$(Bi_{0.5}K_{0.5})TiO_3$–$BaTiO_3$ lead-free ceramics, *Int. J. Appl. Ceram. Technol.*, 8(2011), No. 2, p. 423.

[9] J. Shieh, K.C. Wu, and C.S. Chen, Switching characteristics of MPB compositions of $(Bi_{0.5}Na_{0.5})TiO_3$–$BaTiO_3$–$(Bi_{0.5}K_{0.5})TiO_3$ lead-free ferroelectric ceramics, *Acta Mater.*, 55(2007), No. 9, p. 3081.

[10] R. Sumang, D.P. Cann, N. Kumar, and T. Bongkarn, The influence of firing temperatures on the crystal structure, microstructure and dielectric properties of $0.68Bi_{0.5}Na_{0.5}TiO_3$–$0.22Bi_{0.5}K_{0.5}TiO_3$–$0.10Bi_{0.5}Li_{0.5}TiO_3$Ceramics prepared via the combustion technique, *Ferroelectrics*, 490(2016), No. 1, p. 51.

[11] A. Sasaki, T. Chiba, Y. Mamiya, and E. Otsuki, Dielectric and piezoelectric properties of $(Bi_{0.5}Na_{0.5})TiO_3$–$(Bi_{0.5}K_{0.5})TiO_3$ systems, *Jpn. J. Appl. Phys.*, 38(1999), No. Part1, p. 5564.

[12] D. Maurya, Y. Zhou, Y.K. Yan, and S. Priya, Synthesis mechanism of grain-oriented lead-free piezoelectric $Na_{0.5}Bi_{0.5}TiO_3$–$BaTiO_3$ ceramics with giant piezoelectric response, *J. Mater. Chem. C*, 1(2013), No. 11, art. No. 2102.

[13] K.T.P. Seifert, W. Jo, and J. Rödel, Temperature-insensitive large strain of $(Bi_{1/2}Na_{1/2})TiO_3$–$(Bi_{1/2}k_{1/2})TiO_3$–$(K_{0.5}Na_{0.5})NbO_3$ lead-free piezoceramics, *J. Am. Ceram. Soc.*, 93(2010), No. 5, p. 1392.

[14] P. Bhupaijit, P. Kidkhunthod, S.K. Gupta, N. Nuntawong, S. Prasertpalichat, S. Pinitsoontorn, M. Horprathum, and T. Bongkarn, Phase evolution, microstructure, electrical, and magnetic properties of $Bi_{0.5}(Na_{0.68}K_{0.22}Li_{0.10})_{0.5}TiO_3$ ceramics with Fe^{3+} substitution, *Phys. Status Solidi A*, 217(2020), No. 12, art. No. 1900983.

[15] K. Thangavelu, R. Ramadurai, and S. Asthana, Evidence for the suppression of intermediate anti-ferroelectric ordering and observation of hardening mechanism in $Na_{1/2}Bi_{1/2}TiO_3$ ceramics through cobalt substitution, *AIP Adv.*, 4(2014), No. 1, art. No. 017111.

[16] S. Buntham, P. Boonsong, P. Jaiban, N. Keawprak, and A. Watcharapasorn, Effects of cobalt dopant on microstructure and electrical properties of $Bi_{0.5}Na_{0.5}TiO_3$ ceramics, *Chiang Mai J. Sci.*, 45(2018), No. 6, p. 2481.

[17] B. Parija, T. Badapanda, P. Sahoo, M. Kar, P. Kumar, and S. Panigrahi, Structural and electromechanical study of $Bi_{0.5}Na_{0.5}TiO_3$–$BaTiO_3$ solid-solutions, *Process. Appl. Ceram.*, 7(2013), No. 2, p. 73.

[18] R.Z. Zuo, Z.K. Xu, and L.T. Li, Dielectric and piezoelectric properties of Fe_2O_3-doped $(Na_{0.5}K_{0.5})_{0.96}Li_{0.04}Nb_{0.86}Ta_{0.1}Sb_{0.04}O_3$ lead-free ceramics, *J. Phys. Chem. Solids*, 69(2008), No. 7, p. 1728.

[19] P. Kumar, M. Pattanaik, and Sonia, Synthesis and characterizations of KNN ferroelectric ceramics near 50/50 MPB, *Ceram. Int.*, 39(2013), No. 1, p. 65.

[20] A. Verma, A.K. Yadav, N. Khatun, S. Kumar, R. Jangir, V. Srihari, V.R. Reddy, S.W. Liu, S. Biring, and S. Sen, Structural, dielectric and ferroelectric studies of thermally stable and efficient energy storage ceramic materials: $(Na_{0.5-x}K_xBi_{0.5-x}La_x)TiO_3$, *Ceram. Int.*, 44(2018), No. 16, p. 20178.

[21] X.M. Chen, H.Y. Ma, W.Y. Pan, M. Pang, P. Liu, and J.P. Zhou, Microstructure, dielectric and ferroelectric properties of $(Na_xBi_{0.5})_{0.94}Ba_{0.06}TiO_3$ lead-free ferroelectric ceramics: Effect of Na nonstoichiometry, *Mater. Chem. Phys.*, 132(2012), No. 2-3, p. 368.

[22] A.E.R. Mahmoud, M. Ezzeldien, and S.K.S. Parashar, Enhancement of switching/un-switching leakage current and ferroelec-

tric properties appraised by PUND method of $(Ba_{1-x}Ca_x)TiO_3$ lead free piezoelectric near MPB, *Solid State Sci.*, 93(2019), p. 44.

[23] P.Y. Chen, C.S. Chen, C.S. Tu, P.H. Chen, and J. Anthoniappen, Effects of texture on microstructure, Raman vibration, and ferroelectric properties in $92.5\%(Bi_{0.5}Na_{0.5})TiO_3$–$7.5\%BaTiO_3$ ceramics, *J. Eur. Ceram. Soc.*, 36(2016), No. 7, p. 1613.

[24] U. Obilor, C. Pascual-Gonzalez, S. Murakami, I.M. Reaney, and A. Feteira, Study of the temperature dependence of the giant electric field-induced strain in Nb-doped BNT–BT–BKT piezoceramics, *Mater. Res. Bull.*, 97(2018), p. 385.

[25] Q.H. Zhang, X.Y. Zhao, R.B. Sun, and H.S. Luo, Crystal growth and electric properties of lead-free NBT–BT at compositions near the morphotropic phase boundary, *Phys. Status Solidi A*, 208(2011), No. 5, p. 1012.

[26] I.K. Hong, H.S. Han, C.H. Yoon, H.N. Ji, W.P. Tai, and J.S. Lee, Strain enhancement in lead-free $Bi_{0.5}(Na_{0.78}K_{0.22})_{0.5}TiO_3$ ceramics by $CaZrO_3$ substitution, *J. Intell. Mater. Syst. Struct.*, 24(2013), No. 11, p. 1343.

[27] K.N. Pham, A. Hussain, C.W. Ahn, W.K. Ill, S.J. Jeong, and J.S. Lee, Giant strain in Nb-doped $Bi_{0.5}(Na_{0.82}K_{0.18})_{0.5}TiO_3$ lead-free electromechanical ceramics, *Mater. Lett.*, 64(2010), No. 20, p. 2219.

[28] D.K. Kushvaha, S.K. Rout, and B. Tiwari, Structural, piezoelectric and high density energy storage properties of lead-free BNKT–BCZT solid solution, *J. Alloys Compd.*, 782(2019), p. 270.